Journal of Coordination Chemistry

ISSN: (Print) (Online) Journal homepage: www.tandfonline.com/journals/gcoo20

From germolane to germylenes: a theoretical DFT study of thermal decomposition pathways and reactivity

Ismail Badran

To cite this article: Ismail Badran (14 Nov 2024): From germolane to germylenes: a theoretical DFT study of thermal decomposition pathways and reactivity, Journal of Coordination Chemistry, DOI: 10.1080/00958972.2024.2428799

To link to this article: https://doi.org/10.1080/00958972.2024.2428799

Published online: 14 Nov 2024.

JOURNAL OF COORDINATION CHEMISTRY
https://doi.org/10.1080/00958972.2024.2428799

Taylor & Francis
Taylor & Francis Group

From germolane to germylenes: a theoretical DFT study of thermal decomposition pathways and reactivity

Ismail Badran

Department of Chemistry, An-Najah National University, Nablus, Palestine

ABSTRACT

This study addresses the often-overlooked chemistry of germanium compared to the extensively researched carbon and silicon. Using advanced DFT methods, we investigated the thermal decomposition of germolane (germacyclopentane). The suggested mechanisms include a 1,2-H shift and 1,1-H_2 elimination to form a pentacyclic germylene ($1\lambda^2$-germolane). The other pathway involves a stepwise [3 + 2] cycloreversion to form a diradical followed by ethene and germirane. Under M062X/def2-TZVP level of theory, the activation barriers in terms of Gibbs energy ($\Delta G^{\ddagger}_{298}$) for the 1,2-H shift and 1,1-H_2 elimination pathways were 240.9 and 236.3 kJ/mol, respectively. The reaction energies (ΔG°_{298}) for the initiative steps in the 1,2-H shift and 1,1-H_2 elimination mechanisms were 102.9 and 96.2 kJ/mol, indicating a thermodynamic and kinetic competition between the two routes. Temperature dependence analysis from 300 to 1200 K reveals that the 1,1-H_2 elimination dominates at higher temperatures and is expected to become spontaneous above 1000 K.

GRAPHICAL ABSTRACT

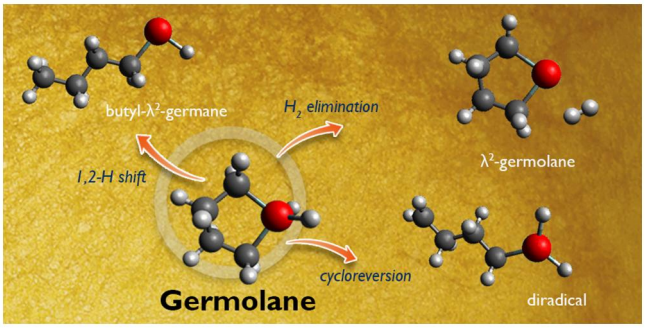

ARTICLE HISTORY
Received 17 September 2024
Accepted 23 October 2024

KEYWORDS
Germolane; germylene; theoretical; DFT; thermal decomposition; reaction mechanism; kinetics

1. Introduction

Unlike the chemistry of carbon and silicon, which has been extensively researched, germanium chemistry has received less attention [1,2]. However, interest in

CONTACT Ismail Badran i.badran@najah.edu Department of Chemistry, An-Najah National University, Nablus, Palestine

germanium and its organic derivatives is on the rise—driven by a variety of applications, including biomedicine, electronics, and catalysis [3–7].

Because it is a good semiconductor, germanium is widely used in the electronics industry, encompassing applications in night-vision devices, infrared optics, and optical fibers [8,9]. Recently, germanium has become important in the development of superconductors and quantum dots [10]. Since inorganic germanium is hydrophobic, it is rarely used in the biomedical industry [5]. Nonetheless, recent attempts to create water-soluble organogermanium compounds have been successful. These substances have physiological, anesthetic, antiviral, antioxidant, and antitumor properties. Particularly, antitumor capability has been demonstrated by germanium sesquioxide [4,9]. Organogermanium compounds have proven their value across different applications, particularly in catalysis [11–13]. For example, Ge-containing compounds have been prepared as redox catalysis, used in the conversion and activation of small molecules, including NH_3, CO_2, CH_4, and H_2 [12,14,15].

Of special interest are divalent species of germanium (germylenes) which are analogues of carbenes [16–18]. The simplest germylene (GeH_2) is a divalent molecule that is widely used as a precursor for the development of Ge-containing thin films *via* chemical vapor deposition (CVD) [19–21]. Many germylenes also exhibit transition-metal-like frontier orbitals on a single site, allowing them to act as efficient catalysts [3]. Germylenes differ from carbenes and silylenes in both their electronic and chemical behavior; while carbenes have typically *triplet* ground states, small germylenes are *singlet*. This is attributed to the strong separation of valence *s*- and *p*-orbitals [3,22]. Also, carbenes and silylenes are very reactive and rarely isolated. In 1999, however, Kira *et al.* isolated the first solid state stable germylene (Scheme 1) in its monomoric form [23]. The title compound (germolane) is inspired by Kira's first germylene.

Despite this growing significance of organogermanium-based catalysis, and germylenes in particular, fundamental research in this area remains limited, leaving many unanswered questions: How does organogermanium chemistry differ from that of carbon and silicon? Do the decomposition mechanisms and reaction kinetics follow similar trends? How do differences in electronic properties of C, Si, and Ge compounds impact their reactivity? These questions motivated us to investigate germolane (Scheme 2), also known as germacyclopentane.

With its unique five-membered heteroatomic structure, germolane offers valuable insights into the chemistry of organogermanium compounds. Furthermore, the 1,1-hydrogen elimination from germolane generates a germylene, formally named $1\lambda^2$-germolane according to IUPAC nomenclature (Scheme 2). $1\lambda^2$-germolane can also be

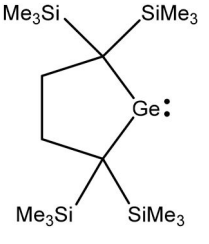

Scheme 1. The first solid state germylene isolated by Kira *et al.* [23].

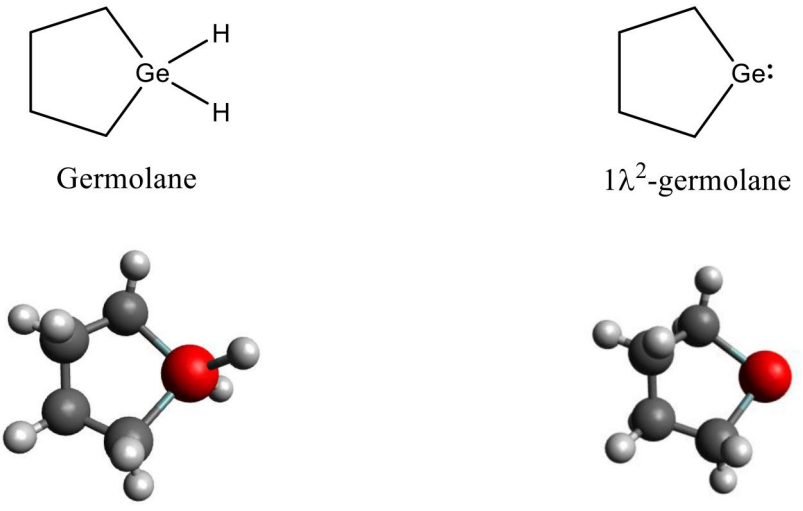

Scheme 2. Molecular structure of germolane and $1\lambda^2$-germolane.

formed upon a 1,2-shift reaction from Ge to C. To the best of our knowledge, there are no prior studies on the reactions of germolane, aside from research on its vibrational spectra [24] and structural parameters [25].

In this work, we employed high-level density functional theory (DFT) to investigate the thermal decomposition of germolane. Specifically, we were interested to explore the 1,1-H_2 elimination and the 1,2-H shift to form $1\lambda^2$-germolane, and the ring opening to form stable olefin species. The functional M062X from the Minnesota group was selected due to its excellent performance in similar studies [26–29]. The def2-TZVP basis set was chosen as recently recommended for similar chemical structures, as well as its ability to describe the electronic structure of the Ge-containing structure [30–35].

This paper is organized as follows: details on the computational methods are provided first, followed by a discussion of germolane decomposition pathways. The discussion includes a thorough examination of the transition states, intermediates, and decomposition products. The mechanism is then analyzed based on the activation energies ($\Delta H^{\ddagger}$ and $\Delta G^{\ddagger}$) and reaction energies (ΔH° and ΔG°). Finally, a thermal analysis that investigates the effect of temperature dependence from 300 - 1200 K is presented.

2. Computational methods

All geometry optimizations were done by employing the M062X functional [36] and the def2-TZVP [37] basis set. This level of theory showed excellent performance in similar studies [26–35]. All species, intermediates, and transition states were optimized using their *singlet* ground states, unless stated otherwise. Frequency calculations were requested after each optimization to ensure that all species exist in their ground states. Transition states (TS) were located either by optimizing educated guesses of their structures, or by performing a relaxed potential energy surface (PES) scan along

the desired reaction coordinate, followed by a TS optimization for the highest point in the PES. All TS were confirmed to have one and only one imaginary frequency along the reaction coordinate. Intrinsic reaction coordinate (IRC) was used to confirm the authenticity of all transition states. No scaling was done for the vibrational frequencies nor the zero-point energies. Enthalpies (H_{298}), Gibbs free energies (G_{298}), and entropies (S_{298}) at room temperature (298 K) were computed as described in our previous work [38–41]. All calculations were done using ORCA 5.03 software [30–35] and viewed in Avogadro [42]. Other graphs were constructed using OriginPro [43]. Data were processed using a user script written by R statistical language [44].

3. Results and discussion

The thermal decomposition of germolane was investigated by exploring different decomposition pathways. This includes a ring opening initiated either by a Ge–C bond rupture or a 1,2-H shift from Ge to the adjacent carbon. The other pathway is hydrogen elimination from the Ge atom to produce a germylene. Herein, the different mechanisms are discussed in detail.

3.1. Mechanism 1: Ring opening via Ge–C bond cleavage

Ring opening in five-membered heterocyclic compounds containing Si and Ge atoms is well known [40,41,45–47]. The ring opening, which can be viewed as a cycloreversion reaction, plays a considerable role in chemistry [48–50]. The reaction can proceed *via* either a [3 + 2] cycloreversion in a concerted single step or a stepwise mechanism initiated by a Ge–C bond rupture followed by another C–C bond rupture to produce at least one olefin.

In the case of germolane, we have not been able to locate a transition state for the concerted [3 + 2] cycloreversion—at least under the level of theory used in this work. From a molecular orbital perspective, [3 + 2] cycloreversion is thermally allowed. However, the nature of the heteroatom and the substituents can dramatically

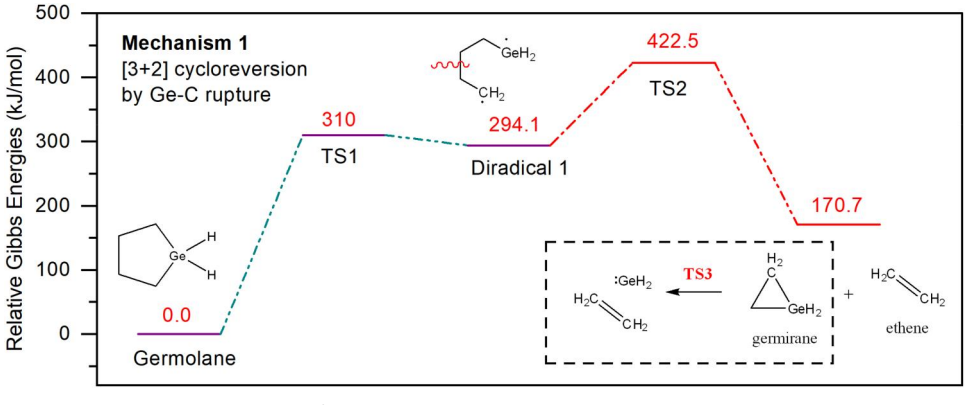

Figure 1. Energy level diagrams for mechanism 1, initiated by a ring opening *via* Ge-C bond cleavage. Values represent Gibbs free energies at room temperature (G_{298}), as obtained at M062X/def2-TZVP level of theory.

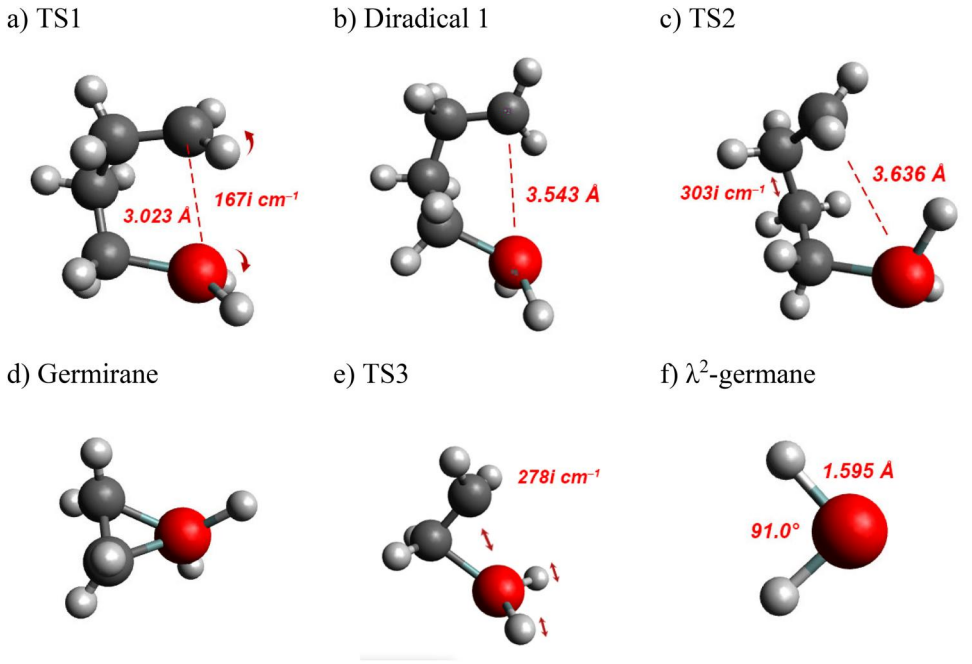

Figure 2. Optimized structures for the transition states, intermediates, and products involved in mechanism 1. Red = Ge atom, gray = C atom, white = H atom. All obtained at M062X/def2-TZVP level of theory.

influence both the symmetry and regiochemistry of the cycloreversion [41,50]. This might explain our inability to locate such TS. Nevertheless, we located the transition state (TS1) for the stepwise route (noted mechanism 1) initiated by a Ge–C bond rupture, as illustrated in Figure 1. An optimized structure of TS1 along with other species involved in this mechanism is shown in Figure 2. Optimized structure of all transition states and stable species involved in this work are also available online free-of-charge in xyz format (see data availability statement). TS1 was characterized by its imaginary vibrational frequency of 167*i* cm^{-1} corresponding to Ge-C bond stretching (Figure 2a). The room-temperature enthalpy of activation ($\Delta H^{\ddagger}_{298}$) and Gibbs free energy of activation ($\Delta G^{\ddagger}_{298}$) of this step were determined to be 309.5 and 310.0 kJ/mol, respectively. As $\Delta G^{\ddagger}_{298}$ encompasses both the enthalpy and entropy components it will be considered for the rest of this discussion. The ring opening through TS1 will yield to the formation of the $\bullet CH_2–(CH_2)_3–GeH_2\bullet$ diradical, as shown in Figure 1. The Gibbs free energy of reaction (ΔG°_{298}) for this step is 294.1 kJ/mol. The value is in close agreement with the reported Ge–C bond dissociation energy (284.0 kJ/mol) in $(CH_3)_3Ge–CH_3$ [51]. It is worth noting that the Ge–C bond length increased from 1.983 Å in germolane to 3.023 Å in TS1 before reaching to 3.543 Å in diradical 1 (*cf.* Figure 2). This agrees with the course of the ring opening of germolane.

Due to its high instability, diradical 1 can decompose further to ethene and germirane through a C-C bond rupture as shown in Figure 1. The decomposition of the diradical proceeds through a transition state (TS2) with an activation barrier $\Delta G^{\ddagger}_{298}$ = 422.5 kJ/mol. As seen in Figure 2c, TS2 has a C-C bond stretching imaginary frequency

of 303*i* cm^{-1} corresponding to the reaction coordinate. The ethene and germirane products lie above the parent germolane molecule by 170.7 kJ/mol; the entire mechanism is endergonic. One could argue that the formation of ethene and germirane from the diradical decomposition should involve both bond dissociation and ring closure, and therefore cannot occur in a single step. Our intrinsic reaction coordinate (IRC) analysis has showed that TS2 does show the formation of a germirane ring, rather than an open-chain dimethylgermane. Because of the very small energy barrier between dimethylgermane and germirane, the ring closure proceeds spontaneously.

We also located a transition state (TS3) that connects germirane to ethene and λ^2-germane (the simplest germylene). Interestingly, our success in finding this transition state contrasts with the suggestion that this reaction proceeds without a barrier [23]. The decomposition of germirane has a $\Delta G^{\ddagger}_{298}$ and ΔG°_{298} of 32.4 and 58.9 kJ/mol, respectively. It was also found that the decomposition through TS3 is endothermic ($\Delta H^{\circ}_{298} = 32.4$ kJ/mol). This agrees with the fact that addition reactions for similar systems are usually exothermic [40,46,52]. The low values of $\Delta G^{\ddagger}_{298}$ and ΔG°_{298} indicate a favorable reaction both thermodynamically and kinetically, which is attributed to weak Ge–C bonds in cyclic compounds [52]. It is also interesting to observe that ethene can be a product of two termination steps in this mechanism, and therefore is expected to be a major product of germolane thermal decomposition. One of the termination products of mechanism is λ^2-germane (GeH_2). Figure 2f depicts the optimized structure with a Ge–C bond distance of 1.595 Å and a nearly right angle of 91.0° between H–Ge–H. The values are consistent with the reported values of 1.593 Å and 91.3 degrees [19].

3.2. Mechanism 2: Ring opening via 1,2 H-shift

The ring opening in germolane can also proceed *via* a 1,2-H shift from the Ge atom to the adjacent C atom as depicted in Figure 3 (mechanism 2). The reaction forms another germylene, namely, butyl-λ^2-germane, through a transition state TS4. The transition state is identified by an imaginary frequency of 1196*i* cm^{-1}, which shows H

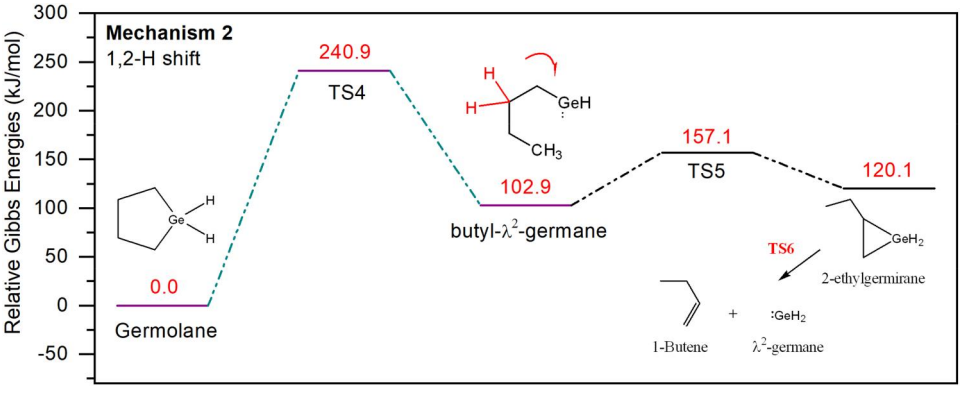

Figure 3. Energy level diagrams for mechanism 2, initiated by a ring opening *via* 1,2-H shift. Values represent Gibbs free energies at room temperature (G_{298}), as obtained at M062X/def2-TZVP level of theory.

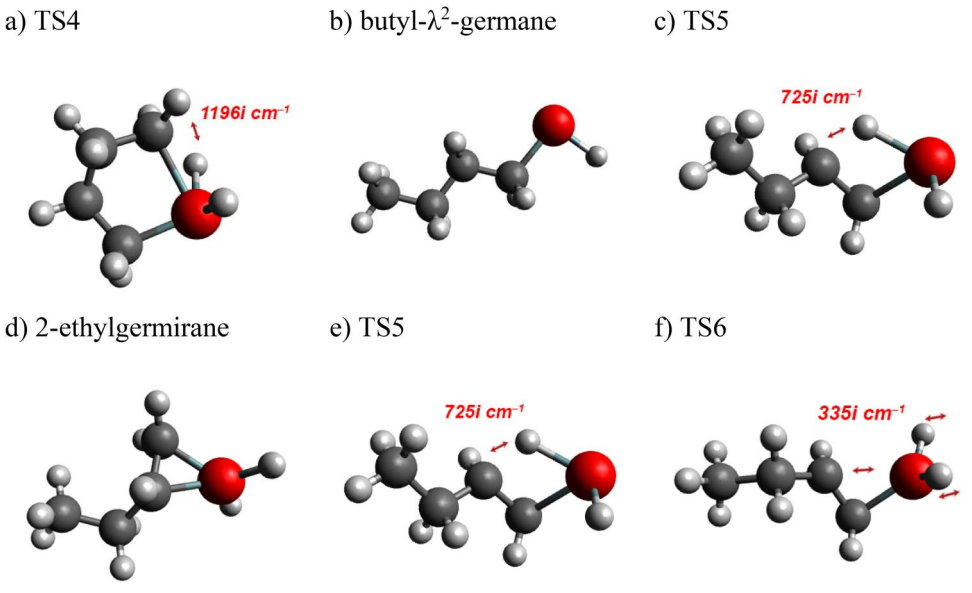

Figure 4. Optimized structures for the transition states, intermediates, and products involved in mechanism 2. Red = Ge atom, gray = C atom, white = H atom. All obtained at M062X/def2-TZVP level of theory.

vibrating towards the adjacent carbon, as seen in Figure 4a. Under the level of theory used in this work, the activation barrier ($\Delta G^{\ddagger}_{298}$) for the 1,2-H shift was 240 kJ/mol. The reaction is also endergonic at room temperature by 102.9 kJ/mol. Thus, the reaction barrier for mechanism 2 is lower than that of mechanism 1, and the product's energy, butyl-λ2-germane, is lower than that of diradical 1. This makes mechanism 2 more kinetically and thermodynamically favorable than the previous mechanism.

Once butyl-λ^2-germane is formed, it can isomerize to 2-ethylgermirane as shown in Figure 3, *via* ring-closing and H-shift. The transition state for this step (TS5, Figure 4c) has an imaginary frequency of 725*i* cm^{-1}. As illustrated in the potential energy diagram in Figure 3, the $\Delta G^{\ddagger}_{298}$ and ΔG°_{298} for the isomerization step are 157.1 and 120.1 kJ/mol, respectively. Clearly, the decomposition of butyl-λ^2-germane is rapid, as the activation barrier between the germylene and TS5 is only 54.2 kJ/mol.

Finally, our calculations revealed that the cyclic product, 2-ethylgermirane, is unstable and can decompose further to 1-butene and GeH_2 (λ^2 germane) through another transition state (TS6). An optimized structure of TS6 is shown in Figure 4f. The activation barrier ($\Delta G^{\ddagger}_{298}$) and the reaction energy (ΔG°_{298}) of the last step were 152.3 and 49.1 kJ/mol, respectively, based on the energy of 2-ethylgermirane.

3.3. Mechanism 3: 1,1-H_2 elimination

Figure 5 shows a third mechanism for germolane's thermal decomposition, as explored at M062X/def2-TZVP level of theory. A concerted 1,1-H_2 elimination from the Ge atom can occur through a transition state TS7, resulting in the formation of 1λ^2-germolane—plus H_2 molecule. TS7 (Figure 6a) has an imaginary frequency of 1216*i* cm^{-1} that clearly shows H-H stretching towards the formation of H_2 molecule. The

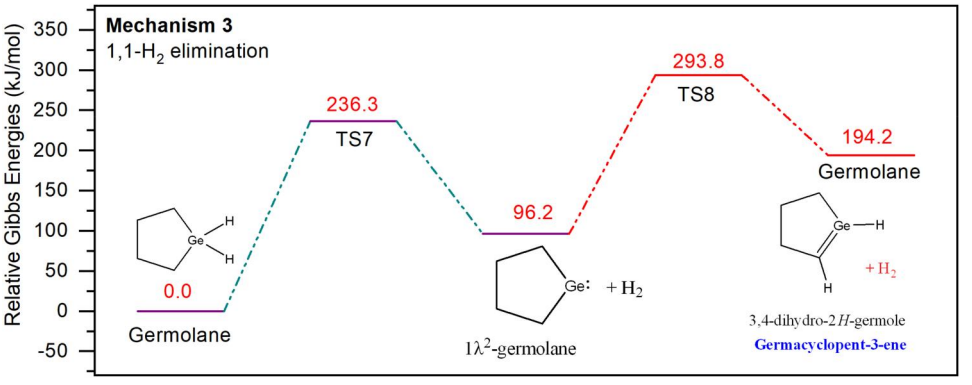

Figure 5. Energy level diagrams for mechanism 3, initiated by 1,1-H_2 elimination from germolane. Values represent Gibbs free energies at room temperature (G_{298}), as obtained at M062X/def2-TZVP level of theory.

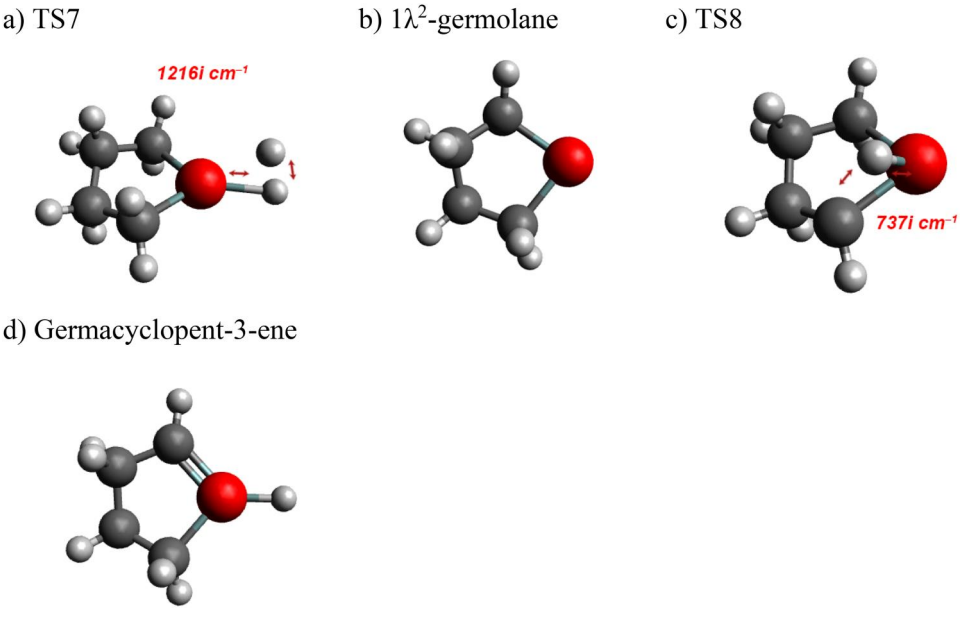

Figure 6. Optimized structures for the transition states, intermediates, and products involved in mechanism 3. Red = Ge atom, gray = C atom, white = H atom. All obtained at M062X/def2-TZVP level of theory.

optimized structures for the transition states and species involved in mechanism 3 are shown in Figure 6. Under our level of theory, the calculated $\Delta G^{\ddagger}_{298}$ and ΔG°_{298} for 1,1-H_2 elimination are 236.3 and 96.2 kJ/mol, respectively. The first activation barrier in 1,1-H_2 elimination is close to that of 1,2-H shift (mechanism 2). Similarly, the values of ΔG°_{298} for the formation of butyl-λ^2-germane (mechanism 2) and $1\lambda^2$-germolane (mechanism 3) are close to each other. This suggests that, at least at room temperature, mechanisms 2 and 3 compete. In our previous work on silacyclobutanes [40,41,53,54], we observed a similar trend between concerted H_2 elimination and 1,2-H shift in silicon-containing cyclic compounds to form silylenes.

According to our third mechanism, germylene ($1\lambda^2$-germolane) is indeed unstable and can undergo isomerization through a 1,2-H shift forming a double bond in germacyclopent-3-ene. The last step proceeds through TS8, which has an imaginary frequency of 737*i* cm^{-1}. The optimized structures for the transition state and the cyclic olefin are depicted in Figure 6. Compared to the 2nd step in mechanism 2, the formation of germacyclopent-3-ene comes at high energy of $\Delta G^{\ddagger}_{298}$ of 293.8 kJ/mol, and the reaction is endergonic by 194.2 kJ/mol. This makes the possibility of forming germacyclopent-3-ene less likely.

3.4. Thermal analysis and temperature dependence

In the previous sections, we discussed the thermal decomposition of germolane *via* three different routes. The discussion was based on changes in enthalpy (ΔH_{298}) and Gibbs free energy (ΔG_{298}) at room temperature. We demonstrated that all reactions are extremely endothermic as well as endergonic at 298 K. This makes sense because the thermal decomposition of organic molecules is typically not spontaneous under ambient conditions. In reality, such decomposition occurs at elevated temperatures. To better understand the reaction mechanism and place it in context with experimental data, we repeated the calculations at temperatures from 300 to 1200 K. The vibrational frequencies were recalculated at the same level of theory (M062X/def2-TZVP) at different temperatures in ORCA, and the new enthalpy, Gibbs free energy, and entropy corrections were used to determine the thermodynamic and kinetic parameters at the corresponding temperatures. The calculations were focused only on the first step of each mechanism, because it is the most important for the fate of the reaction. The results of the thermal analysis are shown in Figure 7.

First, the temperature dependence of the enthalpy of activation ($\Delta H^{\ddagger}$) through the transition states (TS1, TS4, and TS7) is shown in Figure 7a. Clearly, increasing the temperature from 300 to 1200 K has little effect on the values of $\Delta H^{\ddagger}$. This is not surprising given the weak temperature dependence of activation barriers when they are expressed in terms of enthalpy. Although the enthalpy of a single molecule increases with temperature due to the rise in heat capacity, the difference in enthalpy tends to cancel out between the reactant and the TS [41,55,56].

By comparison, the Gibbs free energy of activation ($\Delta G^{\ddagger}$) as a function of temperature is shown in Figure 7b. While $\Delta G^{\ddagger}$ values for the decompaction through TS4 and TS7 tend to show no significant change, the one for TS1 decreases slightly as temperature increases. This can be explained based on two factors: a) the nature of the transition state (loose vs. tight) and b) the reaction temperature. Given that $\Delta G^{\ddagger}$ combines both the enthalpy and entropy terms ($\Delta G^{\ddagger} = \Delta H^{\ddagger} - T\Delta S^{\ddagger}$), and $\Delta H^{\ddagger}$ did not significantly change over the temperature range, and the temperature (T) is fixed for both the reactant and the transition state, the term $T\Delta S^{\ddagger}$ becomes the key factor here. In terms of the optimized structures of the transition states, we can see that TS1 has the most loose structure, allowing it to have higher entropy than TS4 and TS7. As a result, the term $T\Delta S^{\ddagger}$ becomes more negative as temperature increases, resulting in a decrease in $\Delta G^{\ddagger}$.

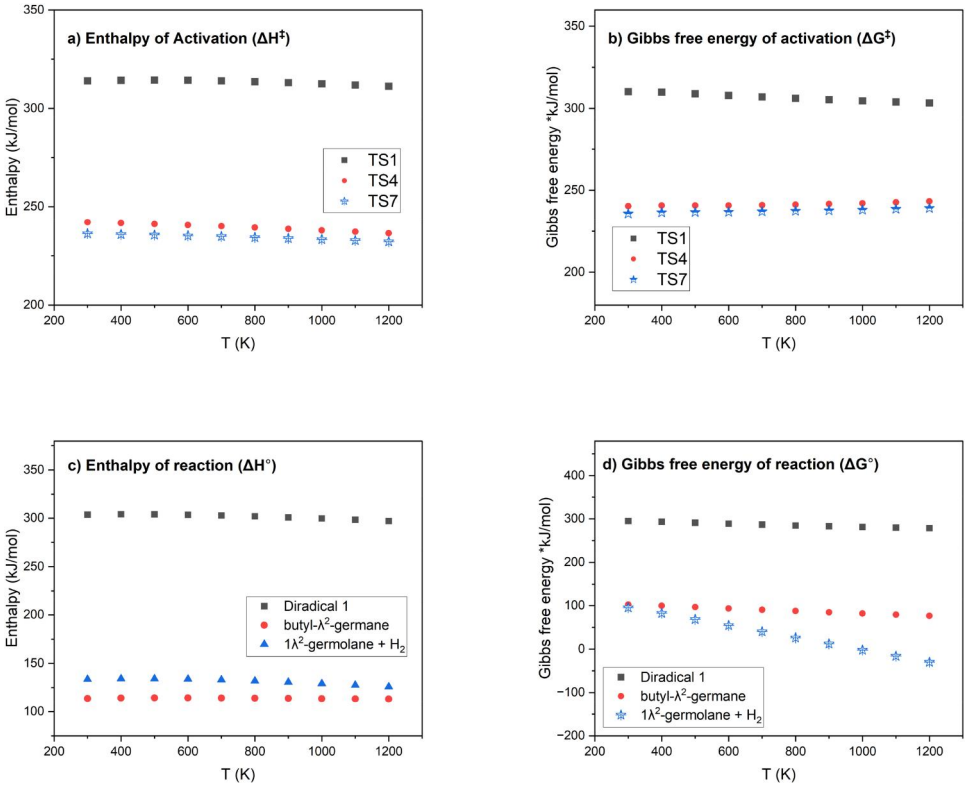

Figure 7. Kinetic and thermodynamic parameters for the thermal decomposition of germolane as a function of temperature. All obtained at M062X/def2-TZVP level of theory.

Next, we present the results of our thermal analysis on the values of ΔH° and ΔG°. The trend of ΔH° did not show a significant change up to 1200 K (Figure 7c). This can be explained on similar grounds that were applied to $\Delta H^\ddagger$. Conversely, the thermal dependence of ΔG° showed a different trend as shown in Figure 7d. The ΔG° values for mechanism 1 (forming diradical) and mechanism 2 (forming butyl-λ^2-germane) remained almost constant with increasing temperature, while ΔG° values for mechanism 3 (forming 1λ^2-germolane and H_2) decreased. This can be rationalized by the changes in translational entropy associated to the formation of two products (mechanism 3) rather than one (mechanisms 1 and 2).

Based on these findings, we conclude that, while mechanisms 2 and 3 compete at room temperature, the decomposition of germolane *via* mechanism 3 (H_2 elimination) becomes more favorable at elevated temperatures, and is expected to be spontaneous around 1000 K.

4. Conclusion

The thermal decomposition of germolane was investigated at the M062X/def2-TZVP level of theory. Three different decomposition pathways were explored including a stepwise cycloreversion initiated by Ge-C bond cleavage, ring opening by 1,2 H-shift, or 1,1-H_2 elimination. The transition state for concerted [3 + 2] cycloreversion could

not be identified at the level of theory used in this study. Rather, germolane cycloreversion proceeds though a stepwise mechanism forming a diradical that decomposes rapidly into ethene and germirane.

The ring opening by 1,2 H-shift led to the formation of an open-chain germylene (butyl-λ^2-germane), which is highly unstable and decomposes quickly to 1-butene and GeH_2. As for the 1,1-H_2 elimination, the reaction forms a cyclic germylene ($1\lambda^2$-germolane) and H_2 molecule. Apparently, $1\lambda^2$-germolane is more stable than the intermediate of the first mechanism (butyl-λ^2-germane) as its isomerization to germacyclopent-3-ene is hindered by a high activation barrier.

The calculations revealed a thermodynamic and kinetic competition between the 1,2 H-shift and 1,1-H_2 elimination routes, which have similar first-step activation barriers and reaction energies.

A thermal analysis was done to investigate the effect of temperature on the reaction mechanism. It was found that the enthalpy term, whether activation barrier ($\Delta H^{\ddagger}$) or reaction energy (ΔH°), were impervious to temperature changes. In contrast, activation ($\Delta G^{\ddagger}$) or reaction energy (ΔG°) in terms of Gibbs free energies show significant changes as temperature increases due to entropy changes. Consequently, it was found that the decomposition of germolane *via* H_2 elimination becomes more favorable as temperature increases, and becomes spontaneous above 1000 K.

Acknowledgements

The author is thankful to the Department of Chemistry and the Faculty of Sciences at An-Najah University for supporting this research. The author also appreciates the developers of ORCA software for making it open source, which facilitated this computational study.

Disclosure statement

No potential conflict of interest was reported by the author(s).

ORCID

Ismail Badran http://orcid.org/0000-0003-1423-7124

Data availability statement

The data that support the findings of this study are openly available in Mendeley Data, V1 at https://www.doi.org/10.17632/4htkntjt36.1

References

[1] O.A. Gapurenko, A.G. Starikov, R.M. Minyaev, V.I. Minkin. *J. Comput. Chem.*, **36**, 2193 (2015).
[2] Y. Liu, S. Zhang, T. Zhu. *ChemElectroChem*, **1**, 706 (2014).
[3] Z. Rappoport. *The Chemistry of Organic Germanium, Tin, and Lead Compounds*, Wiley, Chichester (2002).
[4] L.G. Menchikov, M.A. Ignatenko. *Pharm. Chem. J.*, **46**, 635 (2013).

[5] X. Luo, J. Sun, D. Kong, Y. Lei, F. Gong, T. Zhang, Z. Shen, K. Wang, H. Luo, Y. Xu. *J. Transl. Med.*, **21**, 795 (2023).
[6] I. Haiduc. *J. Coord. Chem.*, **73**, 2117 (2020).
[7] J. Zheng, L. Yang, Y. Deng, C. Zhang, Y. Zhang, S. Xiong, C. Ding, J. Zhao, C. Liao, D. Gong. *Crit. Rev. Environ. Sci. Technol.*, **50**, 1384 (2020).
[8] S. Ng, M. Pumera. *Adv. Mater.*, **35**, 2207196 (2023).
[9] E. Rosenberg. Germanium-Containing compounds, current knowledge and applications. In R.H. Kretsinger, V.N. Uversky, E.A. Permyakov (Eds.), *Encyclopedia of Metalloproteins*, pp. 847–855, Springer, New York (2013).
[10] G. Scappucci, C. Kloeffel, F.A. Zwanenburg, D. Loss, M. Myronov, J.-J. Zhang, S. De Franceschi, G. Katsaros, M. Veldhorst. *Nat. Rev. Mater.*, **6**, 926 (2020).
[11] C. Fricke, G.J. Sherborne, I. Funes-Ardoiz, E. Senol, S. Guven, F. Schoenebeck. *Angew. Chem. Int. Ed.*, **58**, 17788 (2019).
[12] N. Mukherjee, M. Majumdar. *J. Am. Chem. Soc.*, **146**, 24209 (2024).
[13] T. Rogova, E. Ahrweiler, M.D. Schoetz, F. Schoenebeck. *Angew. Chem. Int. Ed.*, **63**, e202314709 (2024).
[14] T. Takeda, S. Doiyama, J. Azumi, Y. Shimada, Y. Tokuji, H. Yamaguchi, K. Nagata, N. Sakamoto, H. Aso, T. Nakamura. *Sci. Rep.*, **9**, 13637 (2019).
[15] R. Gu, X. Feng, M. Bao, X. Zhang. *Nat. Commun.*, **14**, 7669 (2023).
[16] Y. Mizuhata, T. Sasamori, N. Tokitoh. *Chem. Rev.*, **109**, 3479 (2009).
[17] L. Wang, G. Zhen, Y. Li, M. Kira, L. Yan, X.-Y. Chang, L. Huang, Z. Li. *Nat. Commun.*, **13**, 1785 (2022).
[18] F. Suzuki, R. Nishino, M. Yukimoto, K. Sugamata, M. Minoura. *Bull. Chem. Soc. Jpn.*, **93**, 249 (2019).
[19] T.C. Smith, D.J. Clouthier, W. Sha, A.G. Adam. *J. Chem. Phys.*, **113**, 9567 (2000).
[20] I. Badran. *Hot-Wire Chemical Vapour Deposition Chemistry and Kinetics of New Precursors in the Gas Phase and on the Wire Surface*. University of Calgary, Calgary, Alberta, Canada (2014).
[21] I. Badran, T.D. Forster, R. Roesler, Y.J. Shi. *J. Phys. Chem. A*, **116**, 10054 (2012).
[22] W. Kutzelnigg. *Angew. Chem. Int. Ed. Engl.*, **23**, 272 (1984).
[23] M. Kira, S. Ishida, T. Iwamoto, M. Ichinohe, C. Kabuto, K. Ignatovich, H. Sakurai. *Chem. Lett.*, **28**, 263 (1999).
[24] E.C. Thomas, V.W. Laurie. *J. Chem. Phys.*, **51**, 4327 (1969).
[25] G.A. Guirgis, A.M. El Defrawy, T.K. Gounev, M.S. Soliman, J.R. Durig. *J. Mol. Struct.*, **17**, 834–836 (2007).
[26] X. Li, X. Xu, X. You, D.G. Truhlar. *J. Phys Chem. A*, **120**, 4025 (2016).
[27] L. Goerigk, A. Hansen, C. Bauer, S. Ehrlich, A. Najibi, S. Grimme. *Phys. Chem. Chem. Phys.*, **19**, 32184 (2017).
[28] N. Mardirossian, M. Head-Gordon. *Mol. Phys.*, **115**, 2315 (2017).
[29] I.; Badran, K.; Hashlamoun, N.N.; Nassar. *SSRN Elect. J.* (2022).
[30] F. Neese. *WIREs Comput. Mol. Sci.*, **12**, e1606 (2022).
[31] G.L. Stoychev, A.A. Auer, F. Neese. *J. Chem. Theory Comput.*, **14**, 4756 (2018).
[32] G.L. Stoychev, A.A. Auer, R. Izsák, F. Neese. *J. Chem. Theory Comput.*, **14**, 619 (2018).
[33] A. Sen, B. de Souza, L.M.J. Huntington, M. Krupička, F. Neese, R. Izsák. *J. Chem. Phys.*, **149**, 114108 (2018).
[34] M.C.R. Melo, R.C. Bernardi, T. Rudack, M. Scheurer, C. Riplinger, J.C. Phillips, J.D.C. Maia, G.B. Rocha, J.V. Ribeiro, J.E. Stone, F. Neese, K. Schulten, Z. Luthey-Schulten. *Nat. Methods*, **15**, 351 (2018).
[35] F. Neese, F. Wennmohs, U. Becker, C. Riplinger. *J. Chem. Phys.*, **152**, 224108 (2020).
[36] Y. Zhao, D.G. Truhlar. *Theor. Chem. Acc.*, **120**, 215 (2008).
[37] F. Weigend, R. Ahlrichs. *Phys. Chem. Chem. Phys.*, **7**, 3297 (2005).
[38] I. Badran, A. Hassan, A.D. Manasrah, N.N. Nassar. *J. Therm. Anal. Calorim.*, **138**, 1 (2019).
[39] I. Badran, A.D. Manasrah, N.N. Nassar. *RSC Adv.*, **9**, 13403 (2019).
[40] I. Badran, A. Rauk, Y. Shi. *J. Phys. Chem. A*, **116**, 11806 (2012).

[41] I. Badran, A. Rauk, Y. Shi. *J. Phys. Chem. A*, **123**, 1749 (2019).
[42] M.D. Hanwell, D.E. Curtis, D.C. Lonie, T. Vandermeersch, E. Zurek, G.R. Hutchison. *J. Cheminform*, **4**, 17 (2012).
[43] OriginLab Corporation. *OriginPro 9.1: Scientific Data Analysis and Graphing Software*, OriginLab Corporation, Northampton, MA, USA (2019).
[44] RCT. *R: A Language and Environment for Statistical Computing*, R Foundation for Statistical Computing, Vienna, Austria (2024). https://www.R-project.org/.
[45] M. Namavari, R.T. Conlin. *Organometallics*, **11**, 3307 (1992).
[46] L.E. Gusel'nikov. *Coord. Chem. Rev.*, **244**, 149 (2003).
[47] M.S. Gordon, T.J. Barton, H. Nakano. *J. Am. Chem. Soc.*, **119**, 11966 (1997).
[48] E. Opoku, R. Tia, E. Adei. *J. Chem.*, **1**, 4538696 (2016).
[49] E. Opoku, R. Tia, E. Adei. *J. Phys. Org. Chem.*, **32**, e3992 (2019).
[50] S. Bräse. *Synthesis of Heterocycles via Cycloadditions I*, Springer Science & Business Media, Berlin (2008).
[51] Y.-R. Luo. *Comprehensive Handbook of Chemical Bond Energies*, CRC Press, Boca Raton, Florida (2007
[52] R. Koch, T. Bruhn, M. Weidenbruch. *Organometallics*, **23**, 1570 (2004).
[53] I. Badran, Y.J. Shi. *Thin Solid Films*, **595**, 239 (2015).
[54] I. Badran, Y. Shi. *J. Phys. Chem. A*, **119**, 590 (2015).
[55] I. Badran, N.N. Nassar, N.N. Marei, A. Hassan. *RSC Adv.*, **6**, 54418 (2016).
[56] P.W. Atkins, J. De Paula, J. Keeler. *Atkins' Physical Chemistry*, Vol. 14, 11th Edn., p. 441, Oxford University Press, Oxford (2018).